Received May 2001
Revised October 2001
Accepted October 2001

A calculation procedure with multi-block iteration and moving mesh for heat and fluid flows in complex time-dependent geometries

H. Lai and Y.Y. Yan
Department of Mechanical & Manufacturing, The Nottingham Trent University, Nottingham, United Kingdom
J.M. Smith
Department of Chemical & Process Engineering, University of Surrey, Guildford, Surrey, United Kingdom

Keywords *Moving boundary, Iterative methods, Flow, Moving mesh*

Abstract *A calculation procedure is proposed for heat and fluid flows in geometries with a time-dependent boundary. The procedure incorporates a moving mesh arrangement with multi-block iteration and has been developed to assist future simulations of heat and mass transfer with phase change. The solver for the basic equations is the SIMPLE algorithm with a non-staggered grid arrangement. The space conservation law is invoked and applied for the explicit tracking of a moving boundary with a moving mesh. For mapping complex geometries a multi-block iteration strategy is employed. A cubic spline interpolation allows the "uniqueness of zonal boundary" requirement to be met. An interpolation method is also developed for variables near the zone boundaries.*

The calculation procedure using multi-block iteration and a moving mesh is applied to three benchmark-testing problems. The numerical results are in very good general agreement with available experimental data.

Nomenclature

a	= coefficient of discretisation equation (5)	D_{in}	= inner diameter of the annulus in Figure 6
b	= source term of discretisation equation (5)	$\vec{e}_i$	= covariant base of curvilinear coordinates
C_p	= constant-pressure specific heat	g_a	= gravity acceleration
D	= hydraulic diameter of backward facing step in Figure 4	$\sqrt{g}$	= determinant value of metric tensor
		h	= inlet height of the backward facing step in Figure 4

International Journal of Numerical Methods for Heat & Fluid Flow, Vol. 12 No. 2, 2002, pp. 106–125.

DOI 10.1108/09615530210418285

The authors wish to acknowledge the support of EPSRC for this work under grant GR/M90207.

J^{ij} = cofactor of the element in the ith row and jth column in the matrix $(\vec{e}_1, \vec{e}_2, \vec{e}_3)^{\mathrm{T}}$.
$J_{\mathrm{n}}, J_{\mathrm{s}}, J_{\mathrm{e}}, J_{\mathrm{w}}$ = convection-diffusion fluxes at controlling cell face N, S, E and W, respectively. (Figure 2)
K_{eq} = equivalent thermal conductivity
L = radial gap width of the annulus in Figure 6
P = grid node at the centre of control volume
p = pressure
Pr = Prandtl number
q^{ij} = $(J^{im}J^{jm})^{\mathrm{T}}$
R = position vector of P
r = radial
Ra = Rayleigh number
Re = Reynolds number
s = height of the backward facing step in Figure 4 or arc lengths in equation (6)
St = Strouhal number
$S(\phi)$ = source term related to transport variable ϕ in equation (1)
T = temperature
t = time
Δt = increment between time levels
u_{av} = averaged inlet velocity of channel flows
u_i = Cartesian components of Eulerian velocity $\vec{V}$
$u_{g\ i}$ = Cartesian components of mesh velocity $\vec{V}_g$
$\vec{V}$ = Eulerian velocity
$\vec{V}_{\mathrm{g}}$ = mesh velocity
$\vec{V}_{\mathrm{r}}$ = relative velocity defined by equation (2)
W^i_{r} = curvilinear component of relative velocity defined by equation (2)
$X, x_1, x_2, x_3, x_4, x_5, x_6, x_{\mathrm{a}}, x_{\mathrm{b}}$ = horizontal positions defined in Figures 5 or 12
y_i (or x, y) = Cartesian coordinates line
Δy_i = incremental distance in y_i direction

Greek Symbols

ϕ = general transport field variables
Γ_ϕ = diffusion coefficient of ϕ
ρ = density
ν = viscosity
λ = conductivity
β = coefficient of expansion
Ω = volume of control cell
ω = frequency of indentation movement
γ, ε = constants
ξ^i = curvilinear coordinates
$\Delta\xi^i$ = incremental distance in ξ^i direction

Superscripts

i, j, m = free indexes of contravariant component
T = inverse of matrix
* = dimensionless parameters

Subscripts

g = related to mesh
i, j, m = free indexes of covariant component
in, Out = inner and outer cylinder, respectively
$n, n-1$ = time level
NB = neighbour points to node P, i.e. N, S, E, W
n, S, E, w = pertaining cell faces N, S, E, w
P = pertaining to grid point P
r = relative to the moving mesh
I, M, N, Q, R = points in Figure 3

1. Introduction

Heat and fluid flows in complex time-dependent geometries occur in both engineering devices (bubbly flow based reactors, metal materials processors, etc.) and in bio-fluid systems (blood vessels). The conditions often lead to

situations in which flow separation and vortex generation are unavoidable leading inevitably to unsteady heat and flow fields which affect performance.

Many successful strategies and numerical schemes have been developed for simulating heat and fluid flows in time dependent geometries. Most of these have been aimed at the two principal difficulties met in the computations, namely, the tracking of time dependent boundaries and adequate mapping of the complex computational domain. An excellent review of the numerical strategies for tracking time dependent boundaries (often referred as moving boundary problems) has been presented by Shyy *et al.* (1996). Moving boundary tracking can be usually processed by Lagrangian methods such as ALE (arbitrary Lagrangian-Eulerian by Hirt *et al.*, 1974), Eulerian methods such as VOF (Volume of Fluid) method developed by Hirt and Nichols (1981), or Eulerian-Lagrangian methods (the front tracking method of Unverdi and Tryggvason, 1992). However, methods using a moving mesh are always more attractive for studies of local fields because the moving boundary can be explicitly and accurately tracked. In order to map the complex computational domain, which may contain multiply-connected regions which cannot be mapped with a single-grid system, a zoned approach using a composite or overlaid grid system has been developed by Furukawa *et al.* (1991). Computations of heat and fluid flows, not only in multiply-connected regions but sometimes also in a simply-connected region, may be difficult to achieve with a single grid system. For example, using a single grid system to map a spherical-cap or skirted gas bubble surrounded by liquid results in severely skewed grid lines which make calculation difficult. In a zonal approach, the key step is the treatment of the zone boundaries over which the conservation of convection-diffusion fluxes have to be guaranteed. The following treatments have been proposed: the chimera scheme for interpolations on overlaid grids (Benek *et al.*, 1985), Rai's scheme for a TVD (Total Variation Diminishing) finite difference formulation (Rai, 1984), a scheme based on characteristic boundary conditions (Bush, 1985), and the FDM-FEM hybrid scheme (Nakahashi and Obayashi, 1987). Furukawa *et al.* (1991) proposed a zonal approach with non-overlapping structured grids, in which the requirements of uniquely defining the zone boundary satisfying flux conservation across the boundary were met.

In the present paper, moving mesh and multi-block iteration strategies are combined with a zonal approach to calculate heat and fluid flows in complex geometries with moving boundaries. The aim is to develop a reliable and robust algorithm which is intended for the simulation of moving interfacial problems. To the authors' knowledge this approach has not previously been used for the study of interfacial problems.

The present paper is arranged in three sections. Section 2 describes the algorithm. This starts in 2.1 from the basic conservation equations applied to time-dependent heat and fluid flows in a general non-Eulerian co-ordinate frame. The discretisation of the basic equations using a non-staggered SIMPLE algorithm is presented in 2.2, where the "space conservation law" (SCL) is discussed

and used. In Section 2.3, the "uniqueness of zonal boundary" requirement is described and a method of interpolation for the boundary zone is given.

Section 3 presents the performance of the algorithm against three benchmark test problems. These are (a) laminar flow past a backward facing step, (b) natural convection heat transfer in a horizontal annulus, and (c) unsteady channel flow with a moving lateral indentation in the wall. These test problems are presented step by step to demonstrate the robustness of the algorithm and show its potential for future interfacial simulation. Finally the conclusions are summarised in Section 4.

2. Numerical algorithm

2.1 Governing equations

Unless otherwise specified, Einstein's summation law will always apply for any matched free index pairs in the following formulae. In a general non-Eulerian co-ordinate frame $\{t, \vec{e}_i, \xi^i\}$, t is time, $\vec{e}_i$ and ξ^i (i being 1 and 2 for two-dimensional problems and 1, 2 and 3 for three-dimensional questions) are local base vectors and non-orthogonal spatial co-ordinates, respectively. With J^{ij} standing for the cofactor of the element in the ith row and jth column in the matrix $(\vec{e}_1, \vec{e}_2, \vec{e}_3)^T$, $(q^{ij}) = (J^{im})(J^{jm})^T$, and $\sqrt{g}$, the determinant of the metric tensor for the non-Eulerian system, the conservation form of the governing equations for incompressible heat and fluid flow take the following general form:

$$\frac{\partial(\sqrt{g}\phi)}{\partial t} + \frac{\partial(W_r^i \phi)}{\partial \xi^i} = \frac{\partial}{\partial \xi^i}\left(\frac{\Gamma_\phi}{\sqrt{g}} q^{ij} \frac{\partial \phi}{\partial \xi^j}\right) + \sqrt{g} S(\phi), \tag{1}$$

where

$$\phi = \begin{bmatrix} 1 \\ u_i \\ T \end{bmatrix}, \quad \Gamma_\phi = \begin{bmatrix} 0 \\ \nu \\ \dfrac{\lambda}{\rho C_P} \end{bmatrix}, \quad S(\phi) = \begin{bmatrix} 0 \\ -\dfrac{1}{\rho}\dfrac{\partial p}{\partial y_i} \\ 0 \end{bmatrix},$$

T and p are temperature and pressure, respectively, λ, ρ, ν and C_P are fluid properties, u_i the Cartesian components of the Eulerian velocity $\vec{V}$, W_r^i is a curvilinear component of relative velocity $\vec{V}_r$ in the non-Eulerian frame. At a point where the position is $R\rightarrow$, and mesh velocity $\vec{V}_g$, we have:

$$\begin{cases} \vec{V}_r = \vec{V} - \vec{V}_g \\ W_r^i = q^{ij}(u_j - u_{g_j}) = W^i - W_g^i. \\ \vec{V}_g = \dfrac{d\vec{R}}{dt} \end{cases} \tag{2}$$

2.2 Space conservation law and discretisation equations

The application of the space conservation law (SCL) is fundamental to heat and fluid flow calculations using a moving mesh. However, as pointed out by Demirdzic and Peric (1988), although the SCL was discovered by Trulio and Trigger (1961) and "rediscovered" by Thomas and Lombard (1979), its importance has not always been sufficiently realised by researchers. As a result problems have been encountered with oscillations and instabilities, the sensitivity to volume changes and difficulties in pressure iteration.

The SCL is illustrated in Figure 1. For simplicity, a Cartesian co-ordinate cell is employed. The volume of the cell, Ω, is calculated as

$$\Omega = \Delta y_1 \Delta y_2.$$

To calculate the time change rate of Ω using a differential scheme, for example a first-order implicit scheme, we have

$$\frac{\Omega^n - \Omega^{n-1}}{\Delta t} = \frac{[\Delta(\Delta y_1)]^n \Delta y_2^n + [\Delta(\Delta y_2)]^n \Delta y_1^n}{\Delta t}.$$

It is easy to see that the shaded area in Figure 1 has been used twice in calculating the area increase and that this will result in a computational error. The error cannot be avoided by choosing another differential scheme since a similar problem will always be encountered.

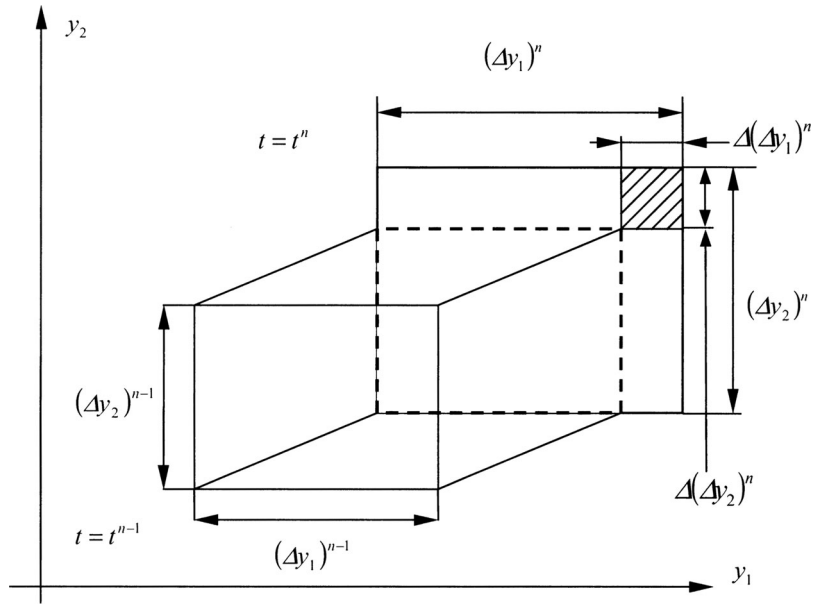

Figure 1.
Space conservation law

In mathematical terms the SCL can be obtained from equation (1) by setting $\phi = 1$, $\Gamma_\phi = 0$, $S(\phi) = 0$ and $\vec{V}_r = -\vec{V}_g$ ($\vec{V} = 0$), which results in:

$$\frac{\partial(\sqrt{g})}{\partial t} = \frac{\partial(W^i_g)}{\partial \xi^i} \tag{3}$$

Equation (3) implies that the time derivative of the computational cell volume is closely related to the grid velocity. To satisfy the SCL, one method is to calculate the grid velocity using equation (2) and then update $\sqrt{g}$ through equation (3). An alternative approach, proposed by Demirdzic and Peric (1988), is to calculate the grid velocity from known grid positions in such a way that the SCL is satisfied. However, in Demirdzic and Peric (1988)'s "general formula" for grid velocity, the projection of the cell face, which might possibly be zero, is used as denominator, which would cause the calculation to fail. For this reason the former method of satisfying the SCL is employed in our paper.

Integrating equation (1) over the shaded control volume shown in Figure 2, we have

$$\frac{(\sqrt{g}\phi)^n - (\sqrt{g}\phi)^{n-1}}{\Delta t}\Delta\xi^1\Delta\xi^2 + J_n - J_s + J_e - J_w = \sqrt{g}S(\phi)\Delta\xi^1\Delta\xi^2. \tag{4}$$

To calculate the cell face fluxes J_n, J_s, J_e and J_w, the first order convection-diffusion schemes (Patankar, 1980) or a high order scheme can be used. In this paper, Van Leer (1979)'s TVD (Total Variation Diminishing) scheme MUSCL (second order in resolution) is employed and implemented in a form of "deferred correction" (Khosla and Rubin, 1974) to the upwind approximation by introducing an additional source term S^ϕ_{DC}. The final form of equation (4) is

$$a_P\phi_P = a_N\phi_N + a_S\phi_S + a_E\phi_E + a_W\phi_W + b + S^\phi_{DC}, \tag{5}$$

where the general dependent variable ϕ at the cell face (denoted by subscript f) between nodes P and $P+1$, is calculated by

$$\phi_f = \begin{cases} \phi_P + \frac{1}{2}\min \mod(\Delta^-_f, \Delta_f), & \text{if } W^i_{r\ f} > 0 \\ \phi_{P+1} - \frac{1}{2}\min \mod(\Delta^+_f, \Delta_f), & \text{if } W^i_{r\ f} > 0 \end{cases},$$

and

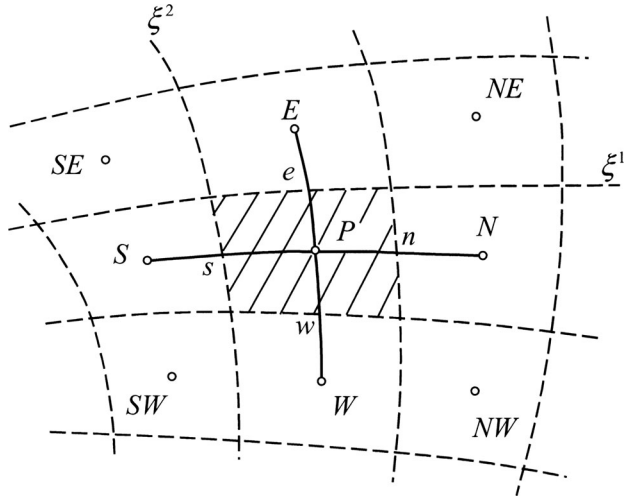

Figure 2.
Control volume for discretisation

$$S_{DC}^{\phi} = \frac{1}{2}\{W_r^1{}_n W_r^{1^+}{}_n \min\ \mathrm{mod}(\Delta_n, \Delta_n^-) - W_r^1{}_n W_r^{1^-}{}_n \min\ \mathrm{mod}(\Delta_n, \Delta_n^+)$$
$$- W_r^1{}_s W_r^{1^+}{}_s \min\ \mathrm{mod}(\Delta_s, \Delta_s^-) - W_r^1{}_s W_r^{1^-}{}_s \min\ \mathrm{mod}(\Delta_s, \Delta_s^+)$$
$$+ W_r^2{}_e W_r^{2^+}{}_e \min\ \mathrm{mod}(\Delta_e, \Delta_e^-) - W_r^2{}_e W_r^{2^-}{}_e \min\ \mathrm{mod}(\Delta_e, \Delta_e^+)$$
$$- W_r^2{}_w W_r^{2^+}{}_w \min\ \mathrm{mod}(\Delta_w, \Delta_w^-) - W_r^2 W_r^{2^-}{}_w \min\ \mathrm{mod}(\Delta_w, \Delta_w^+)\}.$$

The flux limiter is defined by

$$\min\ \mathrm{mod}(A, B) = \mathrm{sgn}(A)\max\{0, \min[|A|, B\mathrm{sgn}(A)]\},$$

$$\Delta_f^- = \phi_P - \phi_{P-1}, \quad \Delta_f = \phi_{P+1} - \phi_P, \quad \Delta_f^+ = \phi_{P+2} - \phi_{P+1}.$$

Employing Rhie and Chow (1983)'s momentum interpolation scheme (also known as a "pressure-weighted scheme") to couple the pressure and velocity, the pressure correction equation, whose form is the same as that of equation (5), can be obtained. The linear equations are solved using ADI iteration methods, and the non-linear equations are solved by the SIMPLE algorithm with a non-staggered grid arrangement.

2.3 Boundary conditions

The boundary conditions related to specific problems will be given in section 3; at this time only the zonal boundary condition is discussed. This includes our treatment of the problem of uniquely defining the zonal boundary together with an appropriate interpolation method. As mentioned in Section 1, both of these serve to guarantee the conservation of convection-diffusion fluxes across the boundary.

Uniqueness of zonal boundary. In the multi-block calculation method, the computational domain is divided into several zones, and grids are generated independently in each zone (block). The zone boundary is defined as the interface between the blocks which have been introduced by the division of the computational domain. Consider the composite multi-block grid system shown in Figure 3. If the zonal boundary is not straight, the independent generation of the grids can cause gaps or overlaps where the boundaries of the two blocks do not coincide. In order to avoid this, Furukawa *et al.* (1991) proposed defining the zonal boundary by the boundary of one block, block 1 in Figure 3 for example. Consequently, the first cell in block 2 connected to the zone boundary is no longer a quadrilateral but a polygon. (That is, in Figure 3, cell *ABCD* is changed into $A'BCD'D''A''A'$). Furukawa *et al.* (1991) further developed an accurate method of high order for evaluating the flux across the zonal boundary. The numerical tests in their paper have demonstrated the potential of the method when applied to complex geometries.

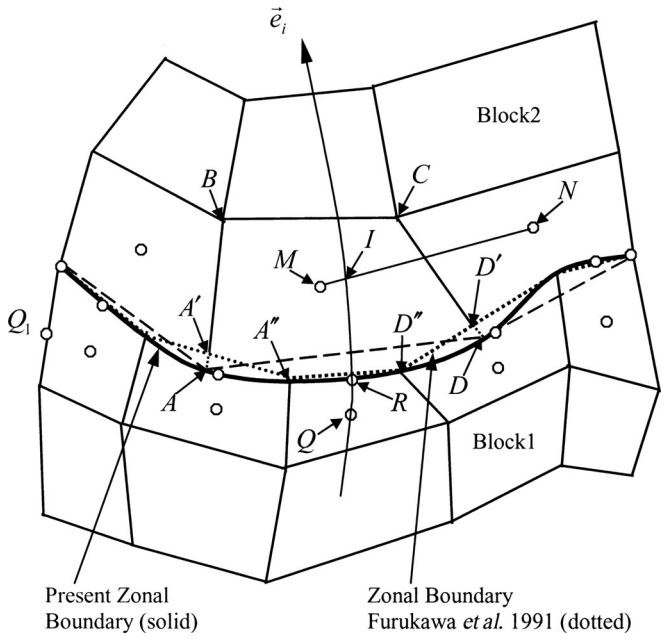

Figure 3.
Multi-block and zonal boundary

However, altering the near boundary cells in block 2 from quadrilaterals to polygons also introduces extra calculation difficulties. Firstly, no single formula is available for the calculation of polygonal cell faces (or cell volumes in three-dimensional problems), and some means is required to identify the complex shape of each cell adjoining the boundary. Secondly, because with a moving mesh the grid speeds for different boundary points are also different, there are extra computational difficulties in defining the topology of polygonal cells.

In this paper, the zone boundary is defined as one of the two blocks as shown in Figure 3. However, in order to guarantee the uniqueness of the boundary, the nodes of block 1, where the mesh has been generated first, are employed to interpolate the boundary nodes of block 2 using a cubic spline interpolation. The topology of the near boundary cells is retained as a "general" quadrilateral with curvilinear sections as the boundaries. In order to calculate the area of the cell, a cubic spline fit is also used to evaluate the determinant of the metric tensor, $\sqrt{g}$; while the cell area is calculated as $\sqrt{g}\Delta\xi^1\Delta\xi^2$. The remainder of the near boundary cell is naturally and understandably treated as a "general" quadrilateral following the basic ideas of body fitted co-ordinates. This application of a cubic spline fit will compensate for the implicit error in the calculation of cell area.

Zonal boundary variable interpolation. In order to solve incompressible flows described by equation (1), boundary values of ϕ are needed. The ϕ at the zone boundary for block 1 is calculated as follows (see Figure 3):

$$\begin{cases} \phi_R^{(1)} = (s_I\phi_Q^{(1)} + s_Q\phi_I^{(1)})/(s_I + s_Q) \\ \phi_I^{(1)} = (s_N\phi_M^{(2)} + s_M\phi_N^{(2)})/(s_N + s_M) \end{cases}, \tag{6}$$

where the numbers in the bracket in the superscripts stand for the blocks, $s_N = \overline{IN}$ and $s_M = \overline{MI}$, $s_I = \overline{RI}$ and $s_Q = \overline{QR}$. The point I is defined as the intersection of the linear segment MN and the extended co-ordinate curve, which passes through point R and outwards from block 1 to block 2.

The $\phi_R^{(1)}$ is used as a boundary value for block 1, and also to evaluate the convection-diffusion flux through the zonal boundary. For block 2, the processing method is similar to that for block 1, and is omitted here. In this paper, flux conservation across the zonal boundary is also imposed according to the method of Furukawa *et al.* (1991).

3. Validation examples

3.1 Backward-facing step problem

The flow over a backward-facing step provides an excellent test case for the accuracy of a numerical method because of the dependence of the reattachment length on Reynolds number. Freitas (1995) recommended the experimental

configuration by Armaly *et al.* (1983) be used as a benchmark problem for algorithm validation. Here we employ it to validate the potential of calculations using a multi-block orthogonal mesh.

The inlet height of the channel is $h = 5.2$ mm, the step height $s = 4.9$ mm. In experiments, the upstream length of the step is nearly 40 inlet heights to ensure the flow is fully developed. Reynolds number is defined as $Re = u_{av} \times D/\nu$, where u_{av} is the averaged inlet velocity, $D = 2h$, $\nu = 1.5 \times 10^{-5}$ (air). In our calculation, the computational domain is divided into upstream and downstream blocks at the step. A fully developed parabolic velocity profile is imposed at 5 step heights upstream of the expansion, and the total length of the computational domain is set at 40 step heights. Non-slip boundary conditions are applied at the top and bottom walls; a uniform static pressure is imposed at the exit boundary. At the zonal boundary, pressure is transmitted upstream from the downstream block, and velocity is transmitted in the opposite direction. Typical grids are illustrated in Figure 4. For block 1 the grid size is 27×54, horizontal $\times$ vertical. For block 2, three mesh sizes, 177×103 (mesh 1), 352×103 (mesh 2) and 452×162 (mesh 3), have been used to evaluate the grid independence of the results for a flow at $Re = 450$. The computed results are given in Figure 5 and Table I.

In Table I the size and location of the separation vortex at $Re = 450$, scaled by the lengths x_1, x_2 and x_3 (see Figure 5 for the definition), calculated by the present method with three different meshes are compared with experiments by Armaly *et al.* (1983). It can be seen that the differences between calculation and experiment are reduced by increasing the grid number, from mesh 1 to mesh 2. For example, the error for x_1 has been reduced by 10.5% (the error for x_1 is 8.5% with mesh 2). This also implies that mesh 1 is not dense enough to get a grid-independent solution. However, further increasing grid density from mesh 2 to mesh 3, gives a reduction of only 0.3% in the error of x_1. It is noted that with this change the error for x_2 even increases by 0.26%, which is about the same as the error reduction for x_1 and may result from experimental deviations will be mentioned later. It is concluded therefore that mesh 2 is dense enough to provide a grid independent solution. At the same time, we observe that the calculated x_1, x_2 and x_3, with mesh 2 or mesh 3, are smaller than their experimental values. Nevertheless these errors are generally smaller than those when commercial CFD codes are tested against the benchmarks as tabulated by Freitas (1995) and perhaps should be accepted.

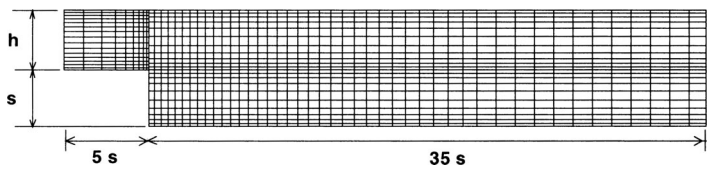

Figure 4.
Illustration of grids distribution for calculation of backward facing step

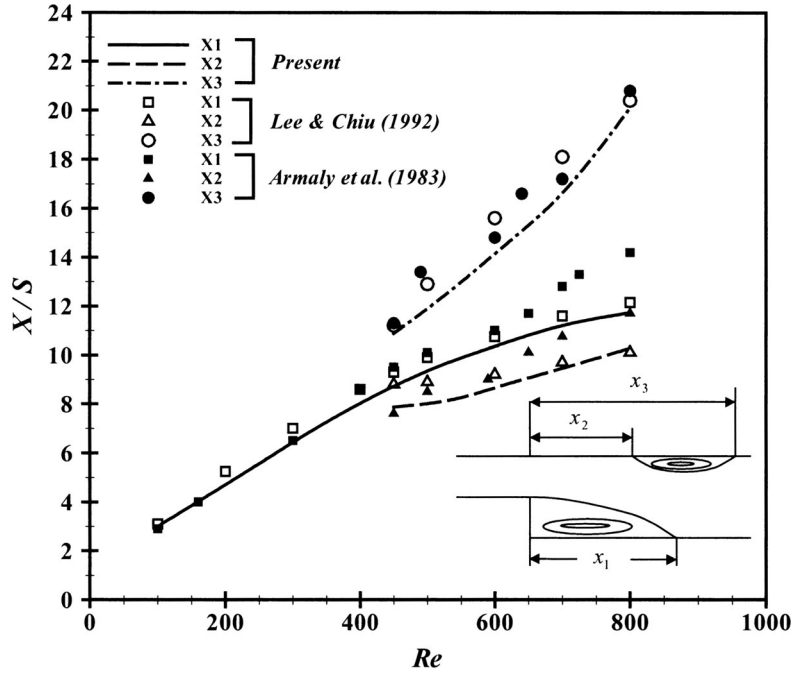

Figure 5.
Positions of reattachment points in a step flow

Figure 5 compares the calculated distributions of x_1, x_2 and x_3, with experiments (Armaly *et al.*, 1983) as Reynolds number is varied. In view of the results presented in Table I, only mesh 2 has been used in getting these distributions. Calculations for different Reynolds numbers are also available in Lee and Chiu (1992), the comparison between their results and the present prediction is also shown in Figure 5, with good agreement up to $Re = 600$, as is also shown for the calculations by Lee and Chiu (1992). At still higher Reynolds numbers the deviation between calculation and experiment becomes steadily larger. As concluded by Kim and Moin (1985) and Freitas (1995), these deviations are not surprising and probably not a result of numerical error, but are more likely to be a result of the apparent three dimensionality and unsteadiness in the measured flow.

Table I.
Reattachment points predicted by three meshes

	x_1	x_2	x_3
Mesh 1	7.69	6.53	10.67
Mesh 2	8.69	7.87	10.88
Mesh 3	8.72	7.89	10.88
Experiment	9.5	7.6	11.3

3.2 Natural convection in horizontal annulus

The second validation test is that of natural convection heat transfer in a horizontal annulus. This calculation demonstrates the use of multi-block non-orthogonal meshes.

The configuration employed here is that of the detailed experimental study by Kuehn and Goldstein (1976) also used for the numerical simulation using SIMPLE algorithm by Date (1986). The value of L/D_{in}(ratio of gap width/inner diameter) is 0.8, the Rayleigh number $Ra = g_a\beta\Delta TL^3/\nu^2$ $Pr = 4.7 \times 10^4$ and the Prandtl number Pr = 0.7. Following the usual methods, as the heat and flow fields are symmetric, half of the concentric annulus, divided along the vertical symmetry line, is employed as the computational domain. In order to validate the robustness of the calculation procedure of using the multi-block body-fitted non-orthogonal mesh, the whole annulus is divided into two non-symmetric blocks as the computational domain (shown in Figure 6). The mesh numbers for the two blocks are 82×52 and 74×42, respectively. Convergence paths for the mass residuals are shown in Figure 7. The computational results are compared with measurements and shown in Figures 8, 9, 10 and 11.

Figure 8 shows the local conductivities at the inner and outer cylinders, defined as follows:

$$K_{eq} = \frac{r \log(r_{\text{out}}/r_{\text{in}})}{T_{\text{in}} - T_{\text{out}}} \frac{\partial T}{\partial r}.$$

Excellent agreement between calculation and experiment is achieved. Even at the near upper symmetry line ($\theta = 0°$) of outer wall, where Date (1986) got a deviation of nearly 1.

The presently computed temperature and angular velocity profiles, also show good agreement with their respective measurements by Kuehn and Goldstein (1976), as shown in Figures 9 and 10. Since the computational blocks are not symmetric, the results in these figures are mean values at the two sides of the geometric symmetry line. In fact, a maximum magnitude of 2 percent for the non-symmetric deviation, defined as the relative deviation of temperature at any two symmetric points, has resulted from the calculation, perhaps because the grids are still not fine enough. As can be seen from Figure 11, very good symmetry for the temperature field and excellent agreement with Kuehn and Goldstein (1976)'s results are obtained in the present calculation.

3.3 Time-dependent moving indentation channel flow

The unsteady channel flow with a time-dependent moving indentation in one wall, which Pedley and Stephanoff (1985) proposed as a benchmark experimental investigation, and to which Ralph and Pedley (1988), Rosenfeld and Kwak (1991) and Lee and Chiu (1992) have derived computed solutions, has been used here to assess the suitability of a multi-block moving mesh for calculation. As shown in Figure 12, the lower wall between x_2 and x_5 is moving

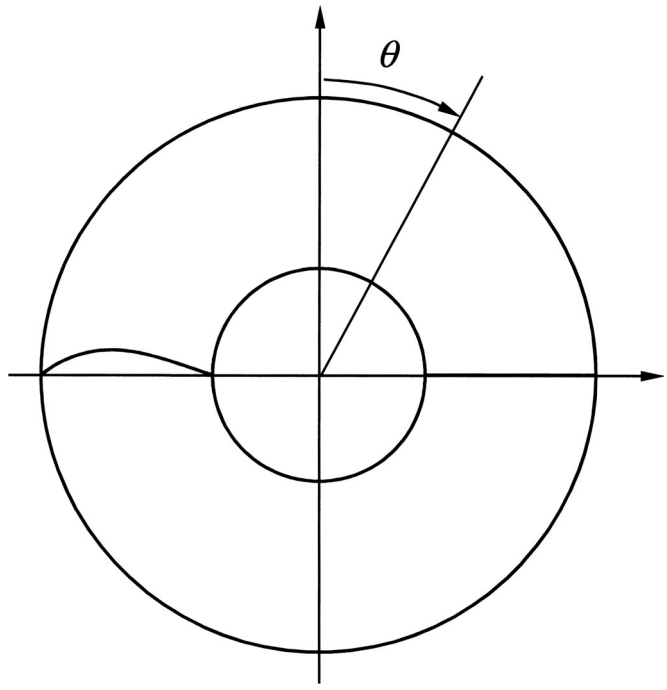

(a) Computational domain

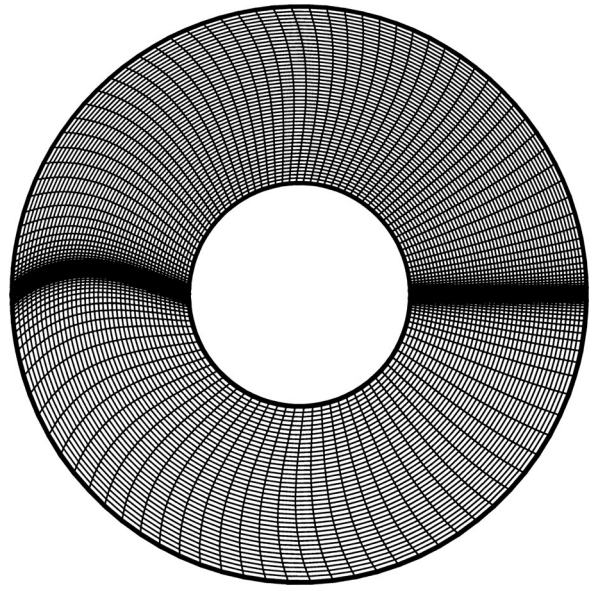

(b) Non-orthogonal grids

Figure 6.
Computational domain and grids for the natural convection in annulus

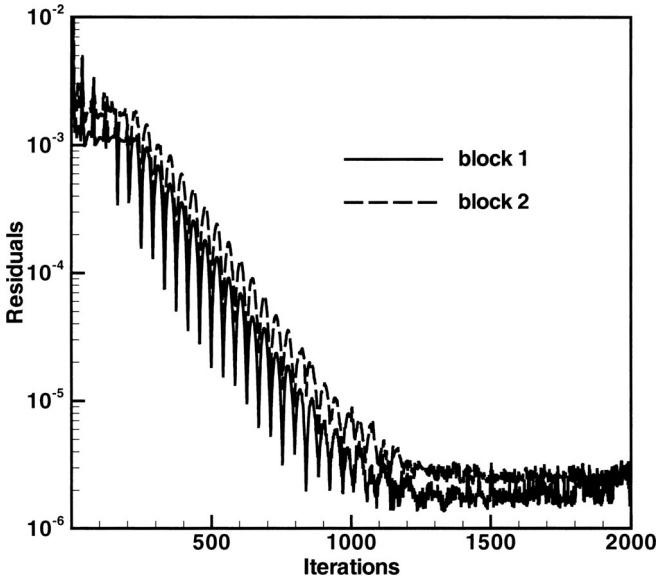

Figure 7.
Convergent path for natural convection in annulus

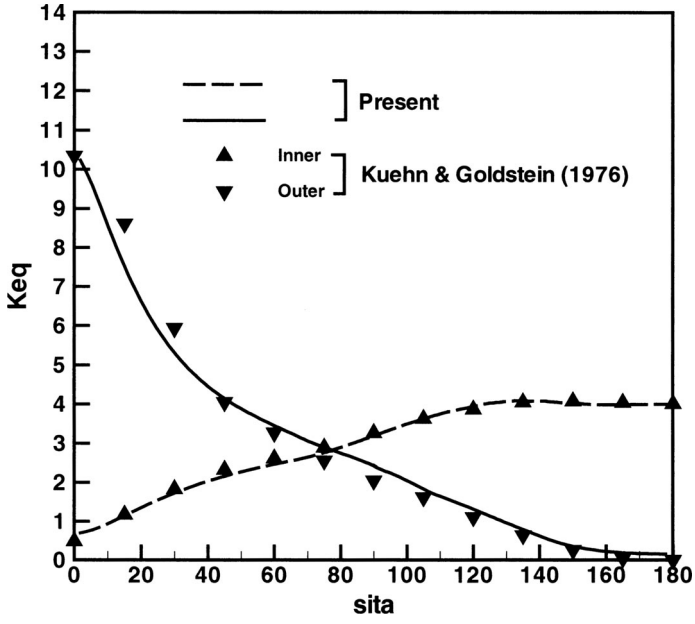

Figure 8.
Local equivalent conductivities at inner and outer walls

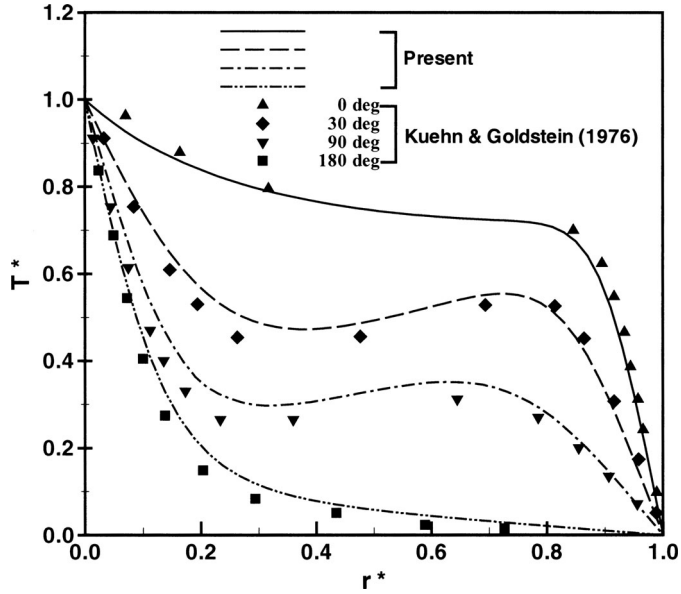

Figure 9.
Temperature profiles

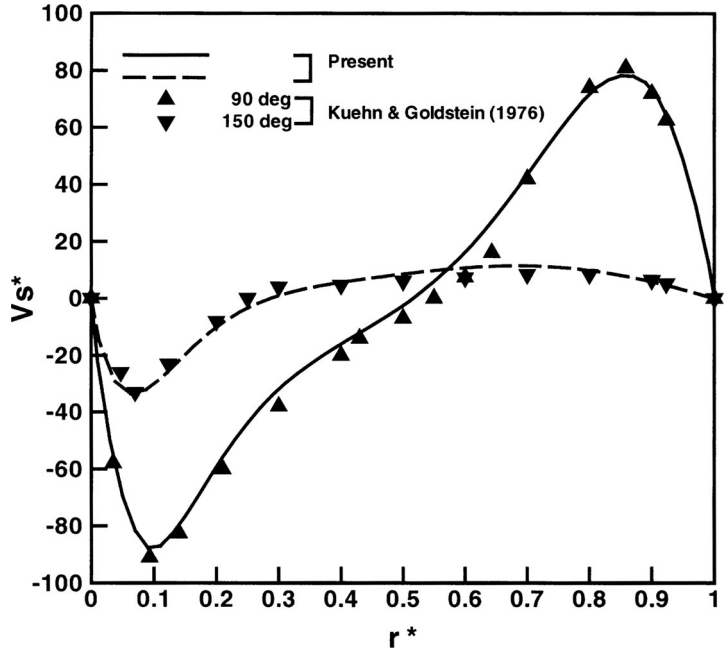

Figure 10.
Distribution of angular velocity

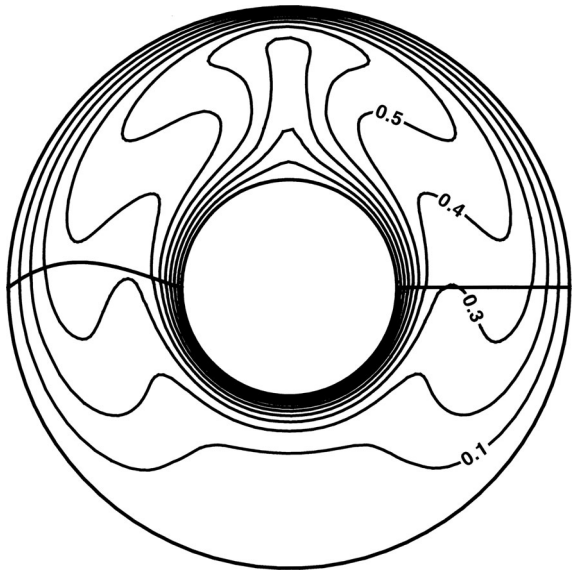

Figure 11.
Contour of non-dimensional temperature

periodically with the vertical co-ordinate $y(x, t)$ defined as following:

$$y(x,\ t^*) = f(x)h(t^*),$$

where $h(t^*) = 0.5(1 - \cos 2\pi t^*)$,

$$f(x) = \begin{cases} 0 & x_1 \le x < x_2 \\ 0.5\varepsilon[1 + \tanh\ \gamma(x - x_a)] & x_2 \le x < x_3 \\ \varepsilon & x_3 \le x < x_4 \\ 0.5\varepsilon[1 - \tanh\ \gamma x] & x_4 \le x < x_5 \\ 0 & x_5 \le x < x_6 \end{cases},$$

$\varepsilon = 0.38$, $\gamma = 4.14$, $x_3 - x_2 = x_5 - x_4 = 2.5$, $x_4 - x_3 = 8$, $x_2 + x_3 = 2x_a$, and $x_4 + x_5 = x_b = 0$. Ralph and Pedley (1988) calculated how the downstream boundary can generally affect the solution up to $(x_6 - x) = 2$. Following their suggestion, $(x_2 - x_1) = 2$ and $(x_6 - x_5) = 12$ are taken as the computational domain in the present paper. In order to evaluate the multi-block calculation, the computational domain has been deliberately divided into two blocks

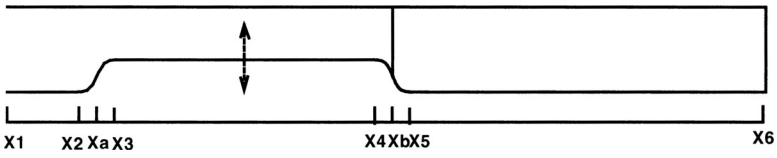

Figure 12.
Computational domain for moving indentation problem

along the vertical position $x = x_b = 0$, as shown in Figure 12. The dimensionless time is defined by $t^* = \omega t$, where t is the dimensional time and ω is the frequency of indentation movement. The Reynolds number based on the averaged inlet velocity u_{av} and the inlet height L is $Re = 507$, while the Strouhal number is $St = L\omega/u_{av} = 0.037$. No-slip boundary conditions are imposed on the top and bottom walls and a fully developed parabolic velocity profile at the inlet, uniform pressure and $\partial\phi/\partial x = 0$ for velocity at exit; The zone boundary is treated in the same way as the backward facing step in Section 3.1. The grid number is 102×52 for block 1 and 177×60 for block 2 with a time step Δt^* of 0.01. The computational results are shown in Figures 13 and 14.

Figure 13 shows the streamlines for a series of instants during one cycle of the indentation movement. The eddy doubling described by Pedley and Stephanoff (1985) is observed around $t^* = 0.6$, when the indentation has reached its top position and is moving downward. With this combination of *Re* and *St* numbers, no obvious vortex shedding is observed in our calculation, which agrees with Lee and Chiu (1992)'s simulation.

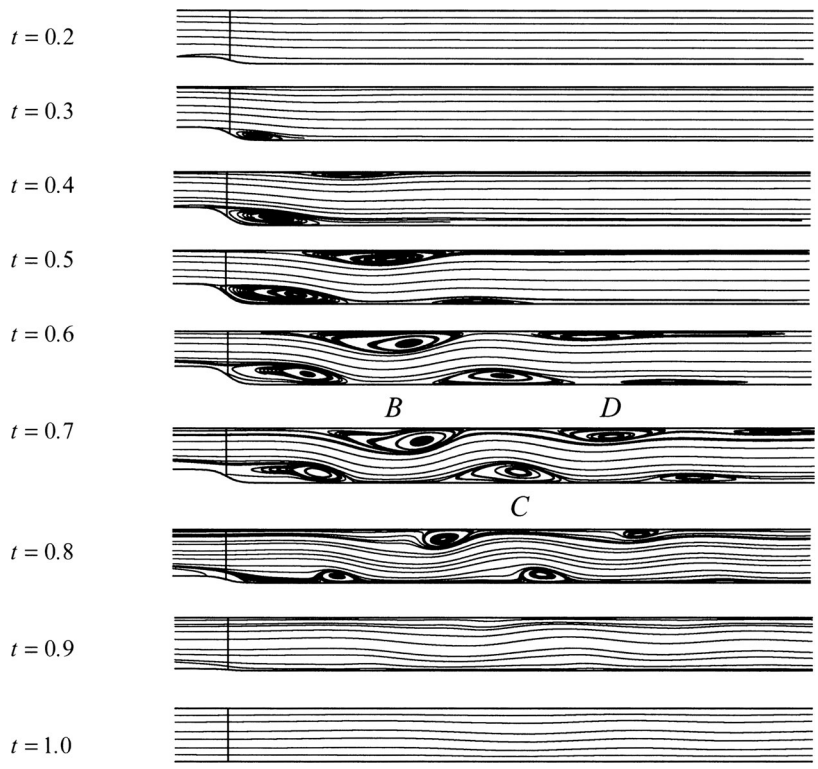

Figure 13.
Stream lines at various instants in a cycle

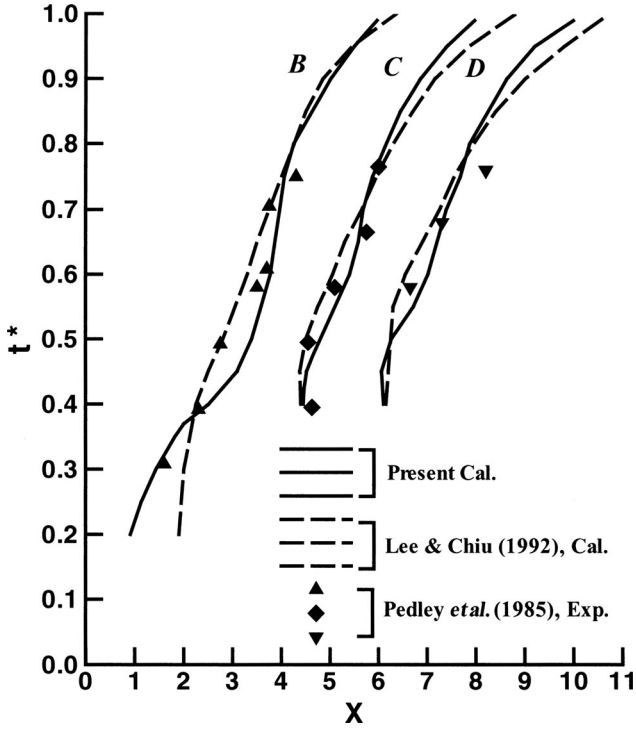

Figure 14.
Positions of the crests and troughs of the eddies

The positions of crests and troughs of the eddies are compared to the experimental results by Pedley and Stephanoff (1985) in Figure 14, where Lee and Chiu (1992)'s computed results are also given for comparison. Although noticeable differences can be found between the simulations of Lee and Chiu (1992) and the present, the overall agreement of both simulations with experiment is reasonable.

4. Concluding remarks

In the present study, a calculation procedure for heat and fluid flows in complex geometries including a time-dependent moving boundary has been put forward. The intention of this paper has been to develop a reliable and accurate algorithm for fluid dynamic simulations requiring the tracking of a moving boundary. We hope in particular that the algorithm will be useful in tracking an interface between two phases.

The calculation procedure incorporates multi-block iteration with a moving mesh, an approach not found in the published literature. The basic equations for fluid flow and heat transfer are solved using the SIMPLE algorithm. In order to use a moving mesh, the spatial conservation law and its application to

the calculations are given; for multi-block iteration, treatments of the zone boundary, including the "uniqueness of zonal boundary" and "zonal boundary interpolation", are suggested.

The computational procedure has been validated step by step by application to three benchmark test problems. These are flow over a backward facing step to validate the application of multi-block calculation to a static Cartesian mesh, natural convection heat transfer in a concentric annulus which has validated the combination of the multi-block approach with a non-orthogonal mesh, and finally, flow in a channel with a moving indentation, which has tested the ability of multi-block moving mesh to solve a more complex time dependent problem. Generally good agreements have been obtained between the present calculations and available experimental data. The calculation procedure has also been shown to be robust.

Future research into multiphase flow and heat transfer will have to consider phase change. Using a zonal boundary approach with an appropriate interpolation scheme for the computational blocks offers useful possibilities for future simulations.

References

Armaly, B.F., Durst, F., Pereira, J.C.F. and Schonung, B. (1983), "Experimental and theoretical investigation of backward-facing step flow", *Journal of Fluid Mechanics*, Vol. 127, pp. 473-96.

Benek, J.A., Buning, P.G. and Steger, J.L., 1985, "A 3-D chimera grid embedding technique", AIAA Paper No. 85-1523.

Bush, R. H., 1985, "External compression inlet predictions using an implicit upwind, multiple zone approach", AIAA Paper No. 85-1521.

Date, A.W. (1986), "Numerical prediction of natural convection heat transfer in horizontal annulus", *International Journal of Heat and Mass Transfer*, Vol. 29 No. 10, pp. 1457-64.

Demirdzic, I. and Peric, M. (1988), "Space conservation law in finite volume calculations of fluid flow", *International Journal for Numerical Methods in Fluids*, Vol. 8, pp. 1037-50.

Freitas, C.J. (1995), "Perspective: Selected benchmarks from commercial CFD codes", *ASME Journal of Fluids Engineering*, Vol. 117, pp. 208-18.

Furukawa, M., Yamasaki, M. and Inoue, M. (1991), "A zonal approach for Navier-Stokes computations of compressible cascade flow fields using TVD finite volume method, ASME", *Journal of Turbomachinery*, Vol. 113, pp. 573-82.

Hirt, C.W. and Nichols (1981), "Volume of Fluid (VOF) Method for the dynamics of free boundaries", *Journal of Computational Physics*, Vol. 39, pp. 201-25.

Hirt, C.W., Amsden, A.A. and Cook, J.L. (1974), "An arbitrary Lagrangian-Eulerian computing method for all flow speeds", *Journal of Computational Physics*, Vol. 14, pp. 227-53.

Khosla, P.K. and Rubin, S.G. (1974), "A diagonal dominant second-order accurate implicit scheme", *Computers and Fluids*, Vol. 2, pp. 207-9.

Kim, J. and Moin, P. (1985), "Application of a fractional-step method to incompressible Navier-Stokes equations", *Journal of Computational Physics*, Vol. 59, pp. 308-23.

Kuehn, T.H. and Goldstein, R.J. (1976), "An experimental and theoretical study of natural convection in the annulus between horizontal concentric cylinders", *Journal of Fluid Mechanics*, Vol. 74, pp. 695-719 Part 4.

Lee, D. and Chiu, J.J. (1992), "Covariant velocity-based calculation procedure with non-staggered grids for computation of pulsatile flows", *Numerical Heat Transfer*, Vol. 21, pp. 269-86 Part B.

Morrison, J.H. and Napolitano, M. (1988), "Efficient solution of two-dimensional incompressible steady viscous flows", *Computational Fluids*, Vol. 16 No. 2, pp. 119-32.

Nakahashi, K. and Obayashi K., 1987, "FDM-FEM zonal approach for viscous flow computations over multiple-bodies", AIAA Paper No. 87-0604.

Patankar, S.V. (1980), *Numerical Heat Transfer and Fluid Flow*, Hemisphere, Washington DC.

Pedley, T.J. and Stephanoff, K.D. (1985), "Flow along a channel with a time-dependent indentation in one wall: The generation of vorticity waves", *Journal of Fluid Mechanics*, Vol. 160, pp. 337-67.

Rai, M.M., 1984, "A conservative treatment of zonal boundaries for Euler equation calculations", AIAA Paper No. 84-0164.

Ralph, M.E. and Pedley, T.J. (1988), "Flow in a channel with a moving indentation", *Journal of Fluid Mechanics*, Vol. 190, pp. 87-112.

Rhie, C.M. and Chow, W.L. (1983), "Numerical study of turbulent flow ast an airfoil with trailing edge separation", *AIAA Journal*, Vol. 21, pp. 1523-32.

Rosenfeld, M. and Kwak, D. (1991), "Time-dependent solutions of viscous incompressible flows in moving coordinates", *International Journal for Numerical Methods in Fluids*, Vol. 13, pp. 1311-28.

Shyy, W., Udaykumar, H.S., Rao, M.M. and Smith, R.W. (1996), *Computational Fluid Dynamics with Moving Boundaries*, Taylor & Francis.

Thomas, P.D. and Lombard, C.K. (1979), "Geommetric conservation law and its application to flow computations on moving grids", *AIAA Journal*, Vol. 17, pp. 1030-7.

Trulio, J.G. and Trigger, K.R., 1961, "Numerical solution of the one-dimensional hydrodynamic equations in an arbitrary time-dependent coordinate system", *University of California Lawrence Radiation Laboratory Report UCLR-6522*.

Van Leer (1979), "Towards the ultimate conservative difference scheme. V. A second-order sequel to Godunov's method", *Journal of Computational Physics*, Vol. 32, pp. 101-36.